Available online at www.sciencedirect.com

ScienceDirect

Ceramics International 40 (2014) 771–777

CERAMICS INTERNATIONAL

www.elsevier.com/locate/ceramint

Characterization of bovine-derived porous hydroxyapatite scaffold and its potential to support osteogenic differentiation of human bone marrow derived mesenchymal stem cells

G. Krishnamurithy[a], Malliga Raman Murali[a], M. Hamdi[b], A.A. Abbas[a], Hanumantharao Balaji Raghavendran[a], T. Kamarul[a,*]

[a]Tissue Engineering Group (TEG), Department of Orthopaedic Surgery, NOCERAL, Faculty of Medicine, University of Malaya, 50603 Kuala Lumpur, Malaysia
[b]Advanced Manufacturing and Material Processing Research Centre, Department of Mechanical Engineering, Faculty of Engineering, University of Malaya, 50603 Kuala Lumpur, Malaysia

Received 5 April 2013; received in revised form 29 May 2013; accepted 19 June 2013
Available online 9 July 2013

Abstract

Porous three-dimensional hydroxyapatite (HA) scaffolds were prepared using bovine cortical bone derived HA (BDHA). Analyses of the morphology, chemical composition, and phase purity of the scaffold were performed using scanning electron microscopy (SEM), micro-computer tomography (micro-CT), Fourier transform infrared spectroscopy (FTIR), energy dispersive X-ray spectroscopy (EDX), and X-ray diffraction (XRD). SEM images revealed the rough and porous surface of the scaffold, while micro-CT showed the average porous volume of $76.7 \pm 0.6\%$ and pore size of 0.04–0.25 mm. Single phase corresponding to standard HA was observed using XRD, and FTIR confirmed the presence of functional groups similar to HA. The EDX analysis revealed a Ca/P ratio of 1.61, which was comparable with HA stoichiometry. Compressive strength of the BDHA scaffold was found to be 1.3 ± 0.09 MPa. After 14 days of human bone marrow stromal cells (hBMSCs) seeding, SEM and confocal analysis revealed cell attachment to the surface and infiltration into the pores. Alamar blue and alkaline phosphatase assays showed significantly increased cell proliferation and differentiation in the BDHA scaffold, when compared with that in the monolayer ($p < 0.01$). In addition, quantitative real-time polymerase chain reaction (qPCR) data confirmed the up regulation of genes involved in osteogenic differentiation of mesenchymal stem cells. Our findings indicate that BDHA scaffold provides a favorable physiological environment for enhanced cell attachment, proliferation, and osteogenic differentiation of hBMSCs.

Keywords: A. Sintering; E. Porosity; Hydroxyapatite; Mesenchymal stem cell

1. Introduction

The use of three-dimensional (3D) scaffolds has been commonly accepted as an essential constituent in bone tissue engineering [1]. As such, various types of scaffolds – natural, synthetic, or a combination of both – have been developed and numerous potential materials for preparing these scaffolds have been introduced. These scaffolds create and maintain space that facilitates progenitor cell migration, proliferation, and differentiation. However, a dispute exists regarding the structural and mechanical properties of scaffolds [2], because the scaffold is expected to remain osteoconductive and subsequently degrade as native tissue forms at the defect region [3]. Current advanced technology in polymer engineering allows fabricating or tailoring synthetic polymer scaffolds such as poly-carbonates-, polyphosphazenes-, polyanhydrides-, and polyethylene glycol (PEG)-based hydrogels to satisfy the needs of bone regeneration [4]. Synthetic polymers such as PLA and PGA have been reported to produce toxic solutions and small particles due to acidic degradation [5]. These small particles trigger an inflammatory response as they are phagocytized by macrophages [6]. In clinical studies where PGA was used as fracture fixation, foreign-body responses or osteolytic reactions have been reported [7,8]. Therefore such issues affect biocompatibility of the implanted material.

*Corresponding author. Tel.: +6019 353 3830.
E-mail address: tkzrea@um.edu.my (T. Kamarul).

0272-8842/$ - see front matter © 2013 Elsevier Ltd and Techna Group S.r.l. All rights reserved.
http://dx.doi.org/10.1016/j.ceramint.2013.06.067

Furthermore, advanced computer-aided design and computer-aided manufacturing (CAD–CAM) technologies have allowed developing 3D design (3-dimension) model of these scaffolds with fine-tuned micro and macroarchitectures [9,10]. Nevertheless, there are issues involved in manufacturing of these scaffolds. First, customized rapid prototyping machine to prepare these bone grafts is very expensive and only available in accredited material engineering centers. Second, the skills and techniques involved in handling this machine are highly advanced and costly. As a result, the cost of the end product is exorbitant, making it available only in affluent medical centers [11]. Therefore, an easily available and cost-effective scaffold material is imperative. Hydroxyapatite (HA), a predominant mineral component of bone, has been widely used as a potential candidate for bone tissue engineering [12]. It is regarded as a biocompatible and biodegradable material because it tends to integrate well into host tissue and degrades over the time without eliciting an immune response [13]. Recently, its application as a scaffold in cell-based therapy has been examined. For the development of a successful scaffold, 3D interconnected porous structure has been reported to be necessary to allow cell attachment, proliferation, and differentiation. Thus, in the present study, we investigated the proliferation and differentiation potential of human bone marrow derived mesenchymal stem cells (hBMSCs) in bovine-derived porous HA (BDHA) scaffold.

2. Experimental

2.1. Fabrication

HA was extracted from the femur of adult bovine bone as described previously [14]. The extracted HA was mixed with 30 wt % commercial sugar (sieved with 300-μm sieve plates to obtain particles of size below 300 μm). The powder mixed with sugar was uniaxially compacted at 156 MPa into green bodies using 10-mm cylindrical dies. Pressureless sintering at atmospheric pressure and ambient humidity was performed on pre-prepared green bodies using a furnace box (Elite Thermal System Ltd., BSF12/6-2408CP) in air atmosphere at 900 °C and ramp rate of 5 °C/min, and dwell time of 2 h. During the sintering process, the green bodies were placed in alumina crucibles (Coors high alumina, Sigma) without covers. The cylindrical BDHA scaffold was used for physicochemical characterization ($n=6$), pore size and porosity characterization ($n=6$), biomechanical ($n=6$), cell attachment ($n=3$), cell culture ($n=8$) and gene expression analysis ($n=8$).

2.2. Characterization

The XRD patterns of BDHA powder were recorded on a D8 Advance X-Ray diffractometer (Bruker-AXS, USA) using Ni-filtered monochromatized CuK_{α} radiation at 40 kV and 40 mA at 25 °C. The diffractogram of HA was found to be correlated with the Joint Committee on Powder Diffraction Standards (JCPDS) diffractogram values of HA (Ca_{10} $(PO_4)_6(OH)_2$) obtained from PDF-4 database (COMBICAT, University of Malaya). High beam of charged particles of approximately 10–30 kV was focused on the specimens using EDX (INCA Energy 200, Oxford Instruments). The number and energy of the X-rays emitted from these specimens were measured by an energy-dispersive spectrometer using Si (Li) crystal detector, and the EDX spectrum was plotted using Micro-analysis Suite software (Version 4.05-Oxford Instruments). For FTIR, BDHA scaffolds were crushed and pressed to obtain thin circular wafer, and the transmission spectra were recorded at 4000–400/cm range. A micro-CT system (SkyScan 1076, Belgium) was used to quantify the 3D microstructural properties of the BDHA scaffold. Isotropic slice data were obtained by the system and reconstructed into two-dimensional images, sliced, compiled, and analyzed to produce 3D images for quantitative architectural parameters [15]. Porosity, pore sizes, and pore distribution were measured from the constructed 3D model.

2.3. Mechanical property

Unconfined isostatic compression test was carried out at a loading speed of 10 mm/min between parallel steel plates using uniaxial compression machine (Instron model 3365, USA). Cylindrical BDHA specimens were prepared with an average dimension of 8.38 ± 0.01 mm (diameter) and 11.86 ± 0.02 mm (height). Stress–strain curve following compression of the BDHA scaffold was generated using Instron software version Blue Hills 2.

2.4. Mesenchymal stem cells culture and assay

hBMSCs were harvested and cultured as described previously [16]. 1×10^6 cells/ml were seeded onto monolayer and porous BDHA scaffold and cultivated with osteogenic medium (Gibco, Invitrogen, USA). Viability assay was carried out based on percentage of alamar blue (AB) reduction on day 0, 3, 6, 9, 12, 15, and 21. Cell attachment was analyzed on day 14 by SEM and confocal microscopy using Hoechst 33342 nuclear stain. Osteogenic differentiation of hBMSCs was measured by alkaline phosphatase (ALP) activity and osteocalcin (OC) secretion on different time points (day 0, 3, 6, 9, 12, 15, and 21).

2.5. Gene expression

The total RNA was isolated from BDHA and monolayer cultures on days 14 and 21 after culturing in osteogenic medium. The RNA isolated from untreated MSCs was considered as a baseline for all the groups. The samples were washed with 1 × PBS and incubated for 4 h in Trizol reagent, and then vortexed vigorously. The supernatants of all the sample groups were collected and the RNA from the collected supernatants was isolated using an RNeasy Mini Kit, according to manufacturer's instructions. Subsequently, 1 μg of RNA was used to generate cDNA using the Superscript III First Strand Synthesis Kit, according to manufacturer's instructions. Primers for alkaline phosphatase (ALP) and osteocalcin (OC) were designed using NCBI database (USA) prior to q-PCR (Table 1). After an initial denaturation step at 95 °C for 3 min, the cDNA products were amplified with 40 PCR cycles, consisting of a denaturation step at 95 °C for 30 s, annealing temperature ranging from 50 to 60 °C, and an extension step at 72 °C for 5 min. The relative quantification values were analyzed using the Bio-Rad CFX manager 2.0. The level of expression of each target gene, normalized

to housekeeping gene, was then calculated as $(1 + E_t)^{\Delta C_t}$, where E_t is the amplification efficiency of the target sequence.

3. Results and discussion

3.1. Characterization

The resolved XRD peaks (Fig. 1A) of both the samples are in accordance with the diffraction pattern of crystalline HA. No additional phase or noticeable differences were observed, indicating that the powder used to produce BDHA scaffold contained single-phase HA with high crystallinity and the sintering process had not altered the composition of HA. It is known that HA consists of several combinations of crystal lattice molecules, such as Ca^{2+}, OH^-, and PO_4^{3-} [17]. The composition of these molecules might vary during fabrication of 3D scaffold and the deviation can be explained by several factors such as different sintering temperature, type of porogen, specific pH value, etc. [18]. The XRD spectrum obtained in the current study correlates with the Bragg peaks of standard HA X-ray diffractogram obtained from JCPDS (9-432). The FTIR spectrum (Fig. 1B) represents the characteristic adsorption peaks of stoichiometric HA (3571.61, 1048.74, 631.86, 601.12, and 570.87/cm) without additional peaks, indicating the absence of chemical decomposition during the sintering process at 900 °C. Furthermore, EDX showed (Fig. 1C) the predominant elements with Ca/P ratio of 1.61, similar to standard HA stoichiometry, which further confirmed that the stoichiometry of HA was retained in the prepared scaffold, as indicated by XRD and FTIR.

Table 1
Forward and reverse primer sequence.

Name	Sequence	Length
ALP		
Forward	CTGGGCTCCAGGGATAAAGC	20
Reverse	TCAGTGTCTCTTGCGCTTGG	20
OC		
Forward	CACACTCCTCGCCCTATTG	19
Reverse	GTCTCTTCACTACCTCGCTG	20
GAPDH		
Forward	TTGATTTTGGAGGGATCTCG	20
Reverse	CAATGACCCCTTCATTGACC	20

3.2. Pore size and porosity

Fig. 2A shows that the scaffolds have an open and porous architecture with porosity of around 76.7 ± 0.6%. Pore size serves as an important morphological factor for tissue

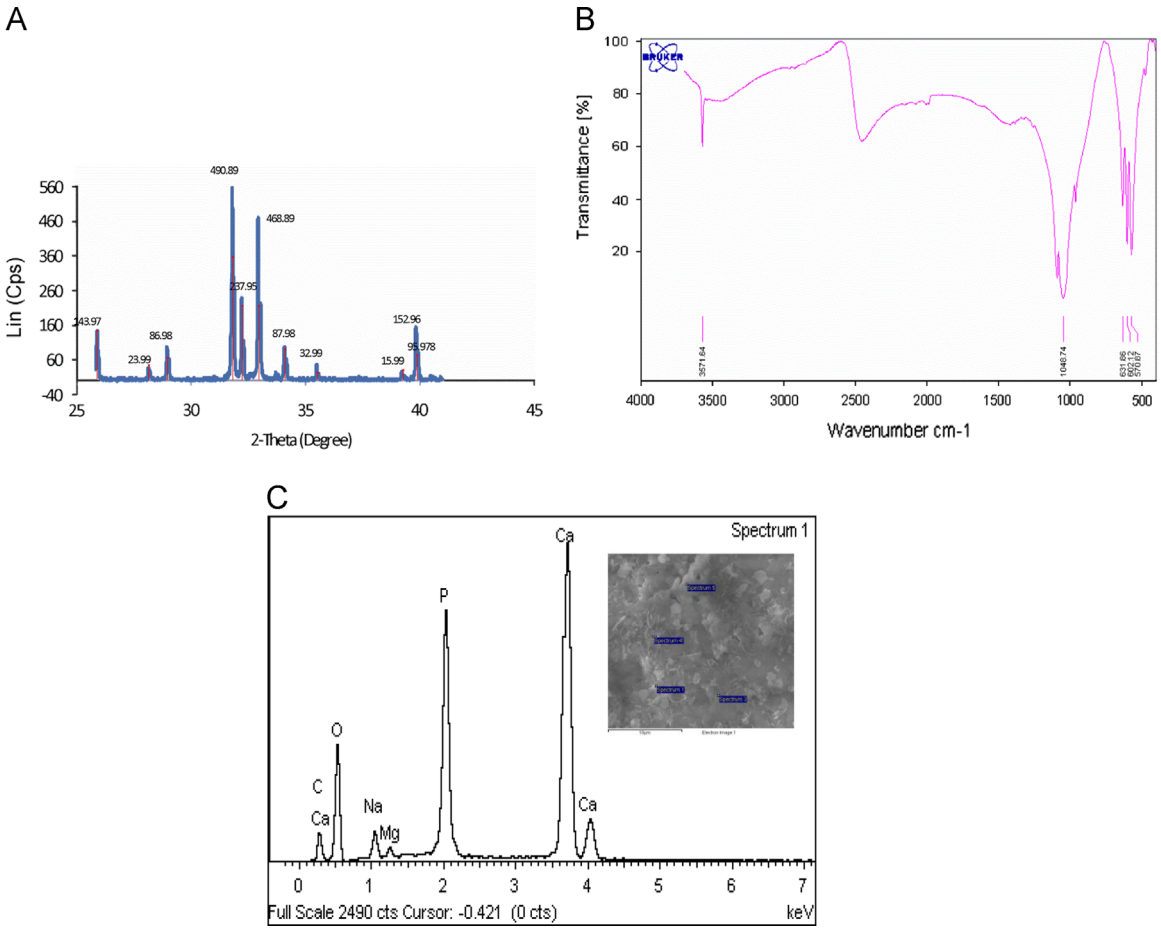

Fig. 1. The physicochemical characteristics of BDHA: (A) XRD pattern compared with the standard HA (red), (B) FTIR spectra, and (C) EDX peaks. (For interpretation of the references to color in this figure legend, the reader is referred to the web version of this article.)

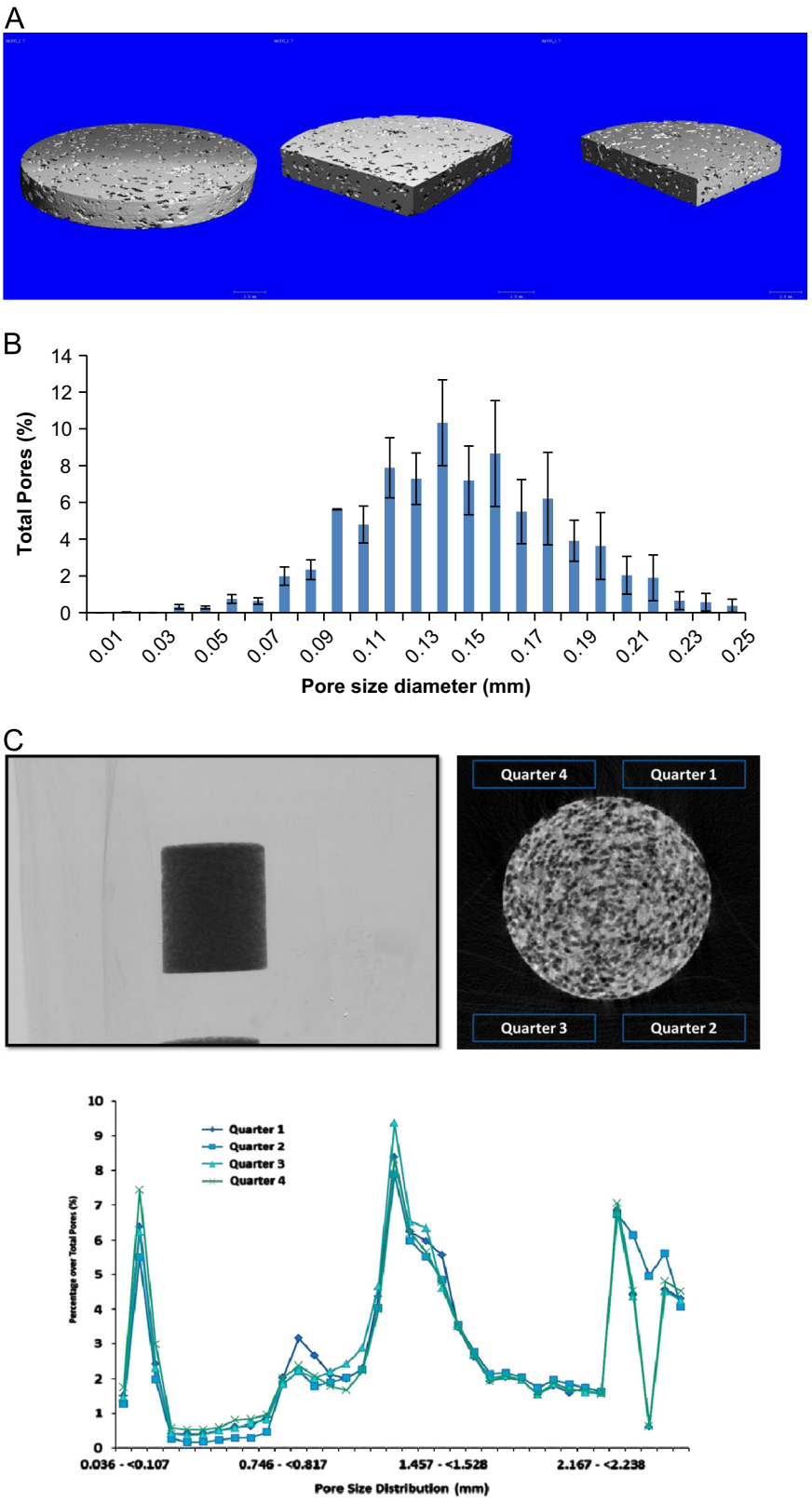

Fig. 2. Micro-CT analysis of BDHA: (A) 3D X-ray images, (B) the total number of pores in percentage against pore size diameter, and (C) the X-ray image of BDHA sectioned into four quarters, and the number of pores (%) vs. pore size.

ingrowth, and in the present study, a broad pore size distribution of 0.04–0.25 mm was observed for BDHA scaffolds (Fig. 2B). These observed pore sizes were found to be in the range of optimal pore size that supports cell growth and internal mineralization. Furthermore, the scaffolds were sectioned into four quarters and the percentage of total pores was

plotted against the distribution of pores according to the sizes (Fig. 2C). The results obtained revealed that the ranges of pore sizes were in equal percentage in all quarters and that there were no significant differences among different quarters.

3.3. Biomechanical analysis

Fig. 3A shows a typical stress–strain response following compression of the BDHA scaffold. The stress increased linearly with an elastic response and failed at a compressive stress of 1.3 ± 0.09 MPa. The data were fitted as a linear equation, $y = mx + c$, and the R^2 value of 0.9902 indicated 99% total variation in the data with regard to the mean.

3.4. Cell attachment

SEM analysis confirmed the porous surface, indicating high affinity of surface for cell attachment. Cells attached to the surface of the scaffold showed flattened morphology (Fig. 3B, Plates 1 and 2), while those infiltrated into pores showed a spherical morphology (Fig. 3B, Plate 3). In addition, the cells were found to extend filopodia (Fig. 3B, Plate 4) to reach the interior pores and also to strengthen the attachment between the cells and scaffold surface. At 1600 × magnification, the architecture around the cells mimic extracellular matrix (ECM) and form continuous layer of fusiform over the surface of the scaffold.

Confocal microscopy on day 14 demonstrated cell attachment and density on the surface of BDHA scaffolds (Fig. 3C, Plate 1) against scaffolds without cells (Fig. 3C, Plate 2). The 3D image obtained from incorporation of multiple series of images collected by confocal laser further assisted the investigation of cell infiltration up to 300 μm into scaffolds (Fig. 3C, Plate 3).

3.5. Cell proliferation and differentiation

The percentage reduction of alamar blue was monitored from day 0 to 21, and the data obtained indicated a significant difference in cell proliferation between BDHA scaffold and monolayer from day 6 to 21 (Fig. 4A). The proliferation rate was also found to be significantly higher in the BDHA scaffold, when compared with that of monolayer ($p < 0.01$). On day 21, a significant increase in ALP production was observed in the BDHA scaffold ($p < 0.01$),

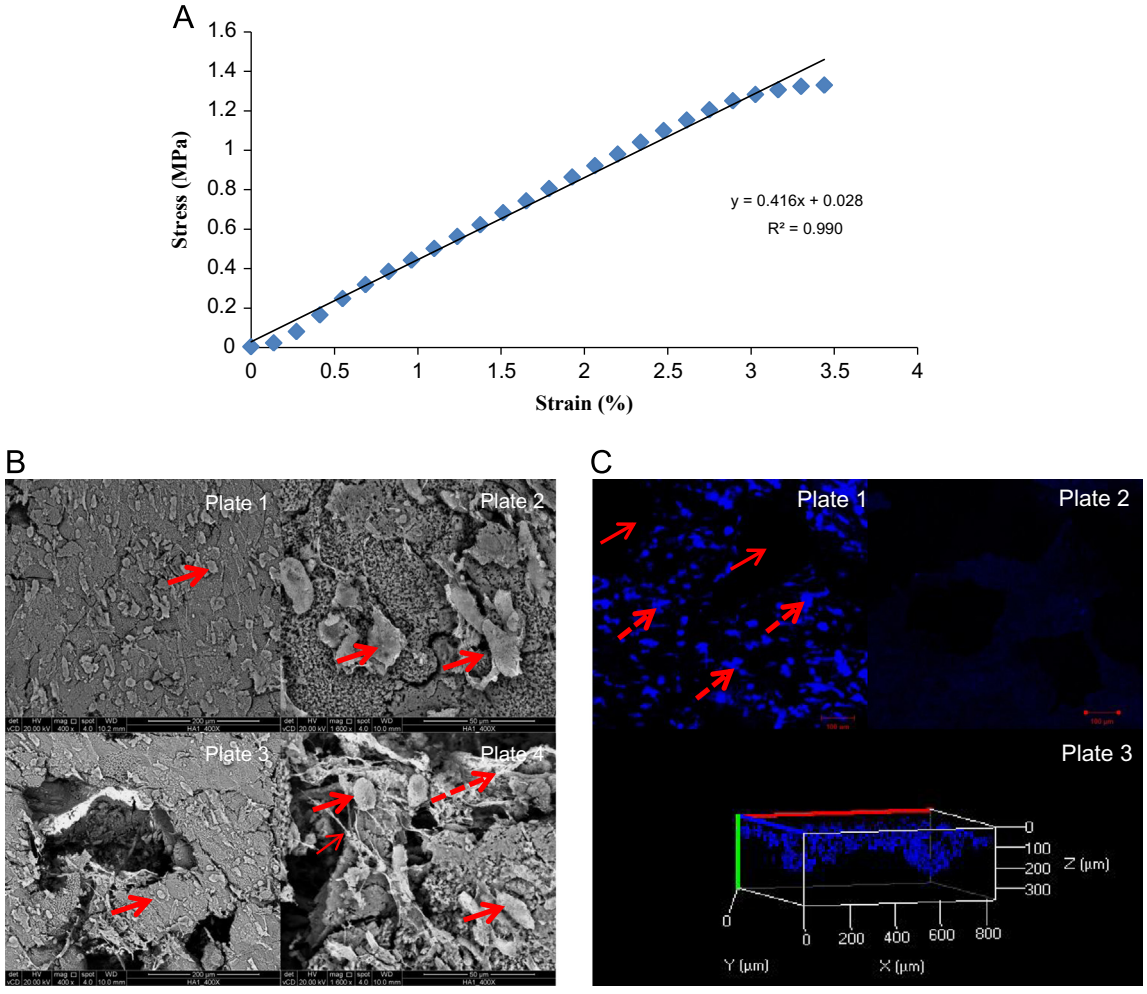

Fig. 3. (A) Stress vs. strain responses, (B) SEM images of cells-BDHA constructs; Plate 1 and 3: 400 × ; Plate 2 and 4: 1600 × ; Cells: ➔, Filopodia: ⟶, ECM: ⇢, and (C) Confocal microscopy images of 100 μm; Plate 1: cell-BDHA constructs; Plate 2: BDHA without cells; Plate 3: 3D image of cells-BDHA constructs. Cells: ⇢ and pores: ➔.

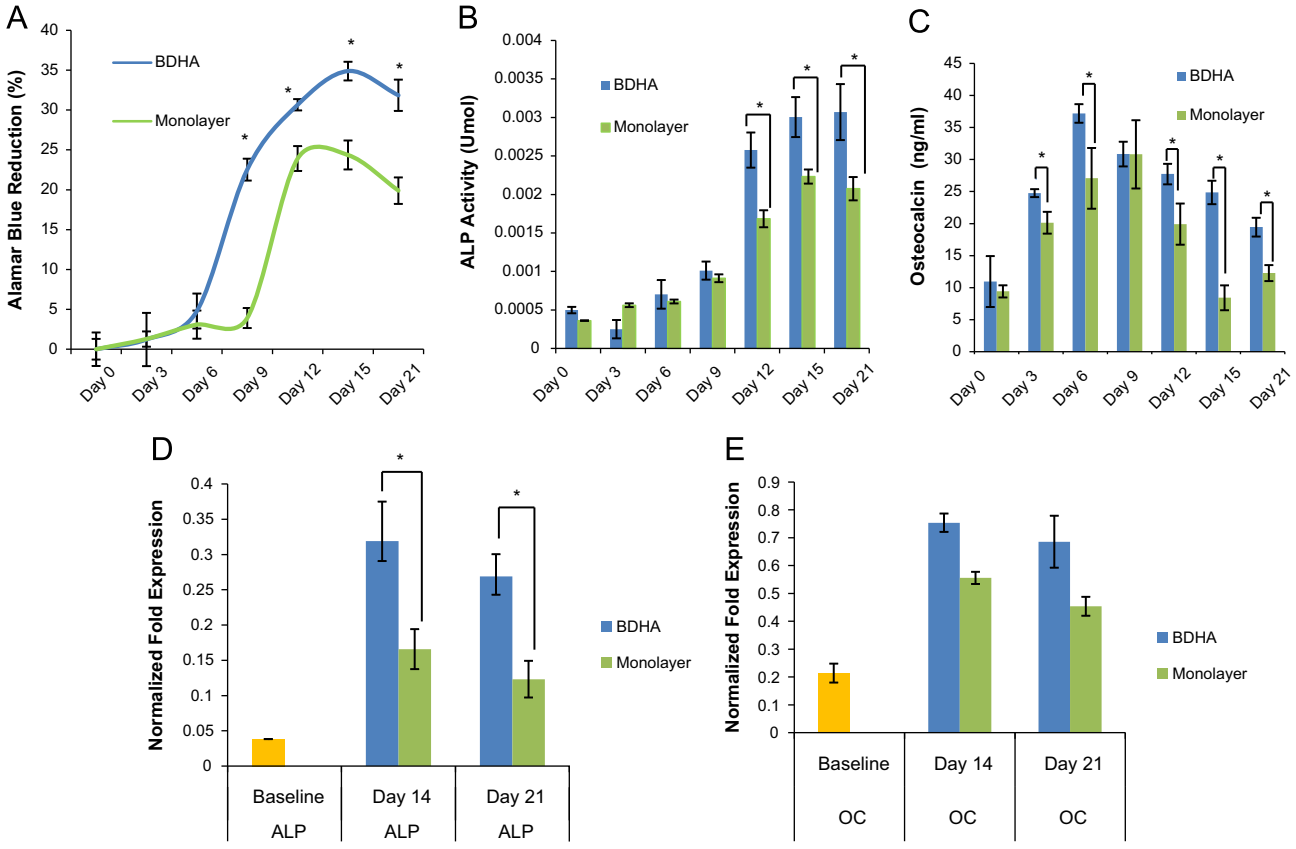

Fig. 4. (A) hBMSC proliferation in porous BDHA scaffold and monolayer – Alamar blue assay, (B) ALP activity of cells grown on porous BDHA and monolayer, (C) OC secretion between BDHA and monlayer, (D) ALP gene expression between baseline (untreated MSCs), BDHA and monolayer and (E) OC gene expression between baseline (untreated MSCs), BDHA and monolayer.*$p < 0.01$ and #$p < 0.05$ was statistically significant when compared to control.

when compared with day 0–9 (Fig. 4B); however, no significant difference in ALP production from day 15 to 21 was observed. Furthermore, substantial difference in ALP production was also observed on day 21 between cells seeded on the BDHA scaffolds and monolayer culture ($p < 0.01$). OC secretion (Fig. 4C) exhibited different trends to that observed for ALP activity. The increased expression of ALP activity indicates enhanced differentiation of MSC to osteoblasts on the scaffolds. Mygind et al. (2007) using coralline scaffolds demonstrated similar findings. They found that the MSCs seeded in 200 μm pore sizes scaffolds increases the ALP activity throughout the 21 days of culture period [19]. Significant increases in OC concentration between day 0 and 6 in BDHA (26.24 ng/ml) and monolayer cultures (17.65 ng/ml) was observed ($p < 0.01$). However, OC secretion was gradually decreased from day 9 onwards in BDHA and day 12 in monolayer. OC secretion BDHA was significantly higher when compared to monolayer cultures ($p < 0.01$). The similar outcome was also reported by Nakamura et al. (2009) in a rat model which demonstrates rat bone marrow derived MSCs seeded on HA scaffolds showed a greater OC secretion compared to monolayer [20].

3.6. Gene expression

Fig. 4D shows the ALP expression in the BDHA and monolayer. The ALP expression in the monolayer culture served as the control. It can be observed that there was a significant increase in the ALP expression in the BDHA and monolayer, when compared with that in the control ($p < 0.01$), possibly due to the progression of osteogenic differentiation of hBMSCs. However, there was no significant increase in the ALP expression in the monolayer. The expression of ALP in the BDHA was significantly higher, when compared with that in the monolayer culture ($p < 0.01$). Similar outcomes have also been reported in another study, in which the MSCs cultured in 200 μm coralline HA expressed a higher degree of ALP [19]. Fig. 4E illustrates the OC expression in the BDHA and monolayer. A significant increase in the OC expression can be observed in the BDHA and monolayer, when compared with that in the baseline ($p < 0.01$). However, there was no significant difference in the OC expression in the BDHA and monolayer between day 14 and 21. It can be noted that the BDHA exhibited higher expression, when compared with the monolayer cultures on days 14 ($p = 0.05$) and 21 ($p = 0.05$). Similar outcomes have also been demonstrated in a previous study that examined BMSCs seeded on HA and commercial scaffolds (BONIT matrix), which reported greater OC gene expression in hBMSCs, when compared with that in the monolayer on plastic surface [21].

4. Conclusion

In conclusion, the results obtained indicate that the BDHA scaffold can be used as a potential functional 3D scaffold for

promoting attachment, proliferation, and differentiation of hBMSCs.

Acknowledgment

The authors are grateful to the University of Malaya research Grant (FP026/2009) and HIR-MOHE for supporting this study.

References

[1] B. Demirbag, P.Y. Huri, G.T. Kose, A. Buyuksungur, V. Hasirci, Advanced cell therapies with and without scaffolds, Biotechnology Journal 6 (2011) 1437–1453.
[2] L. Li, G. Li, J. Jiang, X. Liu, L. Luo, K. Nan, Electrospun fibrous scaffold of hydroxyapatite/poly (ε-caprolactone) for bone regeneration, Journal of Materials Science: Materials in Medicine 23 (2012) 547–554.
[3] T.A. Albrektsson, C.J. Johansson, Osteoconduction and osseointegration, Euroopean Spine Journal 10 (2001) S96–S101.
[4] X. Liu, P.X. Ma, Polymeric scaffolds for bone tissue engineering, Annals of Biomedical Engineering 32 (2004) 477–486.
[5] M.S. Taylor, A.U. Daniels, K.P. Andriano, J. Heller, Six bioabsorbable polymers: in vitro acute toxicity of accumulated degradation products, Journal of Applied Biomaterials 5 (1994) 151–157.
[6] D.F. Gibbons, Tissue response to resorbable synthetic polymers, in: H. Plank, M. Dauner, M. Renardy (Eds.), Degradation Phenomena on Polymeric Biomaterials, vol. 1994, Springer Verlag, New York, 1992 pp. 97–104.
[7] O.M. Bostman, Osteolytic changes accompanying degradation of absorbable fracture fixation implants, Journal of Bone and Joint Surgery, British 73 (1991) 679–682.
[8] O.M. Bostman, Intense granulomatous inflammatory lesions associated with absorbale internal fixation devices made of polyglycolide in ankle fractures, Clinical Orthopaedics 278 (1992) 178–199.
[9] C. Wilson, C. van Blitterswijk, A. Verbout, W. Dhert, J. de Bruijn, Scaffolds with a standardized macro-architecture fabricated from several calcium phosphate ceramics using an indirect rapid prototyping technique, Journal of Materials Science: Materials in Medicine 22 (2011) 97–105.
[10] R. Detsch, F. Uhl, U. Deisinger, G. Ziegler, 3D-cultivation of bone marrow stromal cells on hydroxyapatite scaffolds fabricated by dispense-plotting and negative mould technique, Journal of Materials Science: Materials in Medicine 19 (2008) 1491–1496.
[11] H.L. Greenwood, H. Thorsteinsdottir, G. Perry, J. Renihan, P. Singer, A. Daar, Regenerative medicine: new opportunities for developing countries, Interantional Journal of Biotechnology 8 (2006) 60–77.
[12] S.V. Dorozhkin, Bioceramics of calcium orthophosphates, Biomaterials 31 (2010) 1465–1485.
[13] H. Yoshikawa, N. Tamai, T. Murase, A. Myoui, Interconnected porous hydroxyapatite ceramics for bone tissue engineering, Journal of the Royal Society Interface 6 (2009) S341–S348.
[14] M.K. Herliansyah, D.A. Nasution, M. Hamdi, Ide-Ektessabi, M. W. Wildan, A.E. Tontowi, Preparation and characterization of natural hydroxyapatite: a comparative study of bovine bone hydroxyapatite and hydroxyapatite from calcite, Materials Science Forum 561–565 (2007) 1441–1444.
[15] A.S.P. Lin, T.H. Barrows, S.H. Cartmell, R.E. Guldberg, Microarchitectural and mechanical characterization of oriented porous polymer scaffolds, Biomaterials 24 (2003) 481–489.
[16] S.L. Tan, R.E. Ahmad, T.S. Ahmad, A.M. Merican, A.A. Abbas, W. M. Ng, et al., Effect to growth differentiation factor 5 on the proliferation and tenogenic differentiation potential of human mesenchymal stem cells in vitro, Cells Tissues Organs 196 (2012) 325–338.
[17] S. Joschek, B. Nies, R. Krotz, A. Gopferich, Chemical and physicochemical characterization of porous hydroxyapatite ceramics made of natural bone, Biomaterials 21 (2000) 1645–1658.
[18] L. Chou, B. Marek, W.R. Wagner, Effects of Hydroxyapatite coating crystallinity on biosolubility, cell attachment efficiency and proliferation in vitro, Biomaterials 20 (1999) 977–985.
[19] Tina Mygind, Maik Stiehler, Anette Baatrup, Haisheng Li, Xuenong Zou, Allan Flyvbjerg, et al., Mesenchymal stem cell in growth and differentiation on coralline hydroxyapatite scaffolds, Biomaterials 28 (2007) 1036–1047.
[20] Akifumi Nakamura, Yoshiko Dohi, Manabu Akahane, Hajime Ohgushi, Hiroshi Nakajima, Hiroyuki Funaoka, et al., Osteocalcin secretion as an early marker of in vitro osteogenic differentiation of rat mesenchymal stem cells, Tissue Engineering Part C: Meth 15 (2009) 169–180.
[21] Petra Müller, Ulrike Bulnheim, Annette Diener, Frank Lüthen, Marianne Teller, Ernst-Dieter Klinkenberg, et al., Calcium phosphate surfaces promote osteogenic differentiation of mesenchymal stem cells, Journal of Cellular and Molecular Medicine 12 (2008) 281–291.